Aalto University

Aaltodoc
OPEN ACCESS

This is an electronic reprint of the original article.
This reprint may differ from the original in pagination and typographic detail.

Author(s): Jiang, Hua & Brown, David P. & Nasibulin, Albert G. & Kauppinen, Esko I.

Title: Robust Bessel-function-based method for determination of the (n, m) indices of single-walled carbon nanotubes by electron diffraction

Year: 2006

Version: Final published version

**Please cite the original version:**

Jiang, Hua & Brown, David P. & Nasibulin, Albert G. & Kauppinen, Esko I. 2006. Robust Bessel-function-based method for determination of the (n, m) indices of single-walled carbon nanotubes by electron diffraction. Physical Review B. Volume 74, Issue 3. 035427/1-8. ISSN 1098-0121 (printed). DOI: 10.1103/physrevb.74.035427

Rights: © 2006 American Physical Society (APS). This is the accepted version of the following article: Jiang, Hua & Brown, David P. & Nasibulin, Albert G. & Kauppinen, Esko I. 2006. Robust Bessel-function-based method for determination of the (n, m) indices of single-walled carbon nanotubes by electron diffraction. Physical Review B. Volume 74, Issue 3. 035427/1-8. ISSN 1098-0121 (printed). DOI: 10.1103/physrevb.74.035427, which has been published in final form at http://journals.aps.org/prb/abstract/10.1103/PhysRevB.74.035427

All material supplied via Aaltodoc is protected by copyright and other intellectual property rights, and duplication or sale of all or part of any of the repository collections is not permitted, except that material may be duplicated by you for your research use or educational purposes in electronic or print form. You must obtain permission for any other use. Electronic or print copies may not be offered, whether for sale or otherwise to anyone who is not an authorised user.

# Robust Bessel-function-based method for determination of the $(n,m)$ indices of single-walled carbon nanotubes by electron diffraction

Hua Jiang,[1,*] David P. Brown,[2] Albert G. Nasibulin,[2] and Esko I. Kauppinen[1,2,†]
[1]*VTT Technical Research Center of Finland, P.O. Box 1000, FIN-02044 VTT, Finland*
[2]*NanoMaterials Group, Laboratory of Physics and Center for New Materials, Helsinki University of Technology, P.O. Box 1000, FIN-02044 VTT, Finland*
(Received 5 February 2006; revised manuscript received 22 June 2006; published 26 July 2006)

We report a calibration-free method for the determination of chiral indices $(n,m)$ of single-walled carbon nanotubes from their electron diffraction patterns based on Bessel function analysis of the diffracted layer lines. An approach has been developed for confident identification of the orders of the Bessel functions from the intensity modulations of the diffraction layer lines, to which $(n,m)$ are correlated. In particular, we critically evaluate the effect of nanotube inclination on the validity of the method and show that the layer lines governed by high-order Bessel functions tolerate higher tilt angles than those of low-order Bessel functions and thus are favored for $(n,m)$ evaluation. The method is of particular significance in that it considerably enhances the precision of chiral indexing and makes possible the analysis of high-order Bessel functions, especially when EDPs are of relatively low pixel resolution. The technique can be extended to structural analysis of double-walled carbon nanotubes.

DOI: 10.1103/PhysRevB.74.035427 PACS number(s): 61.14.Lj, 81.07.De

## I. INTRODUCTION

Since their discovery,[1] single-walled carbon nanotubes (SWCNTs) have attracted the attention of the scientific community because of their unique structure and fascinating properties.[2] The properties of carbon nanotubes are extremely sensitive to their atomic structure which is conveniently described by a pair of integers known as the chiral indices $(n,m)$.[2,3] One well-known example is that a nanotube can be metallic if $(n-m)$ is divisible by 3, otherwise they are semiconducting. A slight change in the value $n$ or $m$ can, thus, dramatically alter the electronic properties of a nanotube. For instance, a (13,1) tube is metallic while a (14,1) tube is semiconducting though they are geometrically close to each other.[4] Therefore, an unambiguous $(n,m)$ determination of individual SWCNTs is crucial for the progression of CNT based nanotechnology.

Current efforts for the determination of chiral indices of SWCNTs can be categorized into two broad classes, i.e., optical and nonoptical. Optical spectroscopy includes, for example, resonant Raman scattering[4,5] and photoluminescence.[6] Here, $(n,m)$ are assigned by using the characteristic optical transition energies and photon frequencies (in Raman scattering) or optical absorption and emission energies (in photoluminescence). Optical measurements are usually limited in that they require a range of laser wavelengths for detecting a variety of tubes and they are only valid for a limited range of tube diameters. Laborious efforts are usually involved for both measurement and data interpretation. Photoluminescence has an additional drawback since the method can only detect semiconducting nanotubes. In addition, the insufficient spatial resolution of optical measurement makes it impossible to probe individual SWCNTs for analysis without considering effects from the tube environment. Moreover, there is no known calibration technique to correlate the intensity of excitations for tubes of given chiral indices to their concentrations, thus it is difficult to accurately determine the chirality distribution in a SWCNT sample with optical measurement.

In the nonoptical communities, the chiral indices are usually assigned by first determining the characteristic tube diameter $D_0$ and the chiral angle $\alpha$ by means of direct imaging techniques in real space (such as scanning tunneling microscopy[7,8] (STM) and high-resolution transmission electron microscopy[9] (HRTEM)) or by the electron diffraction technique[1,10–16] in reciprocal space. Direct imaging techniques are faced with the problem that the tubes are usually not stable enough for recording high-quality images with atomic resolution and at a high magnification.

On the other hand, electron diffraction has remained as one of the most attractive means for structural characterization of SWCNTs since their discovery.[1] Advanced nanobeam electron diffraction techniques uniquely allow direct probing of individual nanotubes and the characterization of their structure.[10–13] However, the measurements are typically made by assuming a normal incidence condition[11,12] or a small tube tilting angle, e.g., less than 6°.[15] In contrast, it is not rare for a nanotube to have a tilt angle of 20° from the horizontal plane.[17] In practice, it is difficult to establish an experimental setup to meet such small tilt angle requirements. Although the determination of the chiral angle $\alpha$ from electron diffraction patterns (EDPs) was shown to be independent of tube inclination,[10] evaluation of the tube diameter may rely on the tilt of the tube unless the diffraction patterns are internally calibrated by standard materials, which are in practice unavailable in the measurement. In the absence of such standards, absolute calibration of an EDP of a SWCNT depends on the exact value of the carbon-carbon (C-C) bonding distance, which has an uncertainty between 0.142 and 0.144 nm.[15] Additionally the C-C bond can be stretched when the tube diameter is small.[16] Also, calibration of the EDP by using the C-C bonding distance is either tilt sensitive or complicated by the curvature of the tube. In order to take into account the tilting effect of the tube on the determination, a tedious trial-and-error simulation procedure has been applied.[13]

Moreover, when $D_0$ and $\alpha$ are required to be determined prior to $(n,m)$ assignment, as by previous methods,[1,10,13]

 ©2006 The American Physical Society

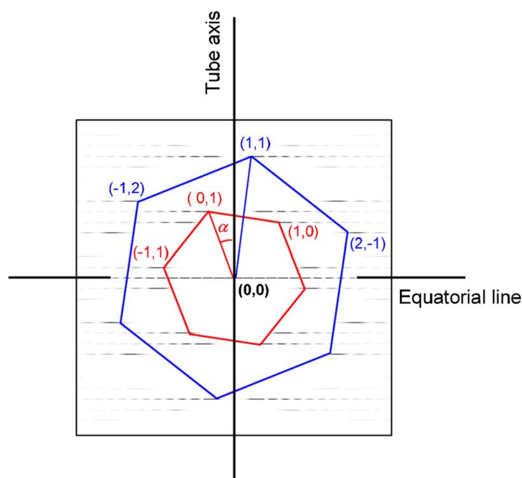


FIG. 1. (Color online) A simulated electron diffraction pattern from a (12,7) chiral SWCNT in normal incidence. The innermost two visible diffraction hexagons from one set of patterns are schematically illustrated, with vertices of hexagons indexed based on the honeycomb lattice structure of a graphene layer.

they must both be determined with high accuracy. A slight error in either $D_0$ or $\alpha$ easily leads to an ambiguity in indexing a SWCNT. For the previously mentioned example, the metallic (13,1) tube has $D_0 = 1.06$ nm and $\alpha = 3.7°$, which is very similar to the semiconducting (14,1) tube with $D_0 = 1.14$ nm and $\alpha = 3.4°$.

Recently Liu and Qin[11] published a Bessel-function-based method which allows the direct assignment of $(n,m)$ to carbon nanotubes based on a unique interpretation of the electron diffraction patterns from the tubes. The orders of Bessel functions that govern the diffraction intensity distributions of the three main layer lines for the graphite {100} reflections are directly ascribed to the chiral indices. The chiral indices are then determined by retrieving the orders of Bessel functions from the corresponding layer line intensity oscillations.

We have independently developed a calibration-free method for a $(n,m)$ determination that is similar to the one reported by Liu and Qin.[11] In this paper, we start with a review of the theoretical basis for such Bessel-function-based methods. Then, we present an approach for the confident retrieval of the orders of the Bessel functions from the intensity modulations of the diffracted layer lines. Importantly, we elucidate the effects of the tube inclination on the validity of the $(n,m)$ determination and demonstrate that the existence of a small tilt angle may lead to the failure of both methods. It is also shown that the layer lines of high-order Bessel functions tolerate higher tilt angles than those of low-order Bessel functions. Recommendations for the proper selection of suitable layer lines for accurate $(n,m)$ evaluations are made. The effectiveness of the proposed method has been demonstrated by a practical example.

## II. THEORETICAL BASIS

Figure 1 shows a simulated EDP of a (12,7) chiral SWCNT in the normal-incidence condition. (If not specified, the electron beam is hereafter assumed to be in normal incidence.) According to the kinematical diffraction theory of carbon nanotubes,[18–22] an electron diffraction pattern of a SWCNT is the superposition of two sets of hexagonal patterns which are produced by the honeycomb lattices on the "top" and the "bottom" graphene layers of the nanotube, respectively. The two sets of patterns are mirrored about the tube axis. Illustrated in Fig. 1 are the innermost two visible diffraction hexagons belonging to one of the two sets of patterns. The vertices of those hexagons are indexed based on the honeycomb lattice structure of the graphene layer.

Due to the effect of the cylindrical curvature of the nanotube, those hexagon vertices are "streaked" in the direction perpendicular to the tube axis. For a $(n,m)$ SWCNT of diameter $D_0$, the intensity distribution along a given streak of the reflection $(h,k)$ is modulated by a particular squared Bessel function (of the first kind), $J_\nu^2(\pi D_0 R)$, where $R$ is the radial distance measured along the layer line from its intersection point with the tube axis $(R>0)$, and $\nu$ is the order of the Bessel function, which is associated with $(n,m)$ by[19]

$$\nu = nh - mk \quad (\nu \text{ is an integer}). \tag{1}$$

To be concise, the squared Bessel function $J_\nu^2(\pi D_0 R)$ is hereafter termed the Bessel factor of order $\nu$. In particular, along the equatorial line at the diffraction center (0,0), the dominant Bessel factor is $J_0^2(\pi D_0 R)$. The dominant Bessel factors for other reflections, such as the (1,0) reflection, is given by $J_n^2(\pi D_0 R)$ with order $n$, the (0,1) reflection by $J_{-m}^2(\pi D_0 R)$ with order $-m$, and the (1,1) reflection by $J_{n-m}^2(\pi D_0 R)$ with order $n-m$.

Note that $\pi D_0 R \geqslant 0$ and $J_{-\nu}^2(\pi D_0 R) = J_\nu^2(-\pi D_0 R) = J_\nu^2(\pi D_0 R)$ due to the symmetry of the Bessel function about its origin and the squaring of the function. A reflection of $J_\nu^2(\pi D_0 R)$ and its mirror counterpart, $J_\nu^2(-\pi D_0 R)$ or $J_{-\nu}^2(\pi D_0 R)$, therefore constitute a distinct diffraction layer line, which is perpendicular to the tube axis. This layer line is thus described by a reduced single Bessel factor $J_{|\nu|}^2(x)$, where the argument $x$ is from $-\pi D_0 R$ to $\pi D_0 R$ and $R$ remains the radial distance measured along the layer line from its intersection point with the tube axis.

It is worth noting that an electron diffraction pattern of a SWCNT is composed of many discrete layer lines. Obviously the layer lines appear only where there are reflections from the honeycomb lattice. It is very possible that more than one reflection takes place in one single layer line. As a consequence, theoretically, contributions to the intensity modulation of this layer line can come from a number of Bessel factors of various orders and the interpretation of the layer line intensity becomes complex. Fortunately, higher order reflections that may occur in the same layer line are usually located far away from the central area of the diffraction pattern and are also negligibly weak. Thus, they do not significantly interfere with the stronger lowest-order Bessel factor contributions and then only one single Bessel factor of the lowest order dominates the intensity distribution of the layer line.

In the case of achiral tubes (zigzag or armchair), there exists no twist angle between the two sets of hexagonal pat-

terns from the top and bottom lattice layers, respectively, hence the two sets of patterns coincide and higher-order reflections appear close to each other in the same layer line and have an interval of $1/d_{100}=4.69\ \mathrm{nm}^{-1}$ for armchair tubes and $\sqrt{3}/d_{100}=8.13\ \mathrm{nm}^{-1}$ for zigzag tubes, respectively. Here $d_{100}=0.213$ nm is the graphite 100 lattice spacing.[2] Even so, the separation between neighboring reflections along one layer line is still large enough for $(n,m)$ characterization.

## III. METHODS

As discussed above, in the normal-incidence condition, the chiral indices $(n,m)$ of a SWCNT are correlated with the orders of Bessel functions (squared) that act as shape factors for the diffraction from the nanotube. This enables the direct evaluation of the chiral indices of carbon nanotubes. The unambiguous determination of $(n,m)$ then depends on reliably retrieving the Bessel orders from the corresponding Bessel factor plots. Liu and Qin[11] used a method to identify the Bessel order by recognizing the characteristic position ratio of the first two positive peaks $(X_2/X_1)$ along a given layer line in the diffraction pattern. Although the authors claimed that, with their method, the chiral indices can be assigned unambiguously up to $(n,m)$ of (30,30), we note that the absolute difference between the value of $X_2/X_1$ for the Bessel factor of order $\nu=9$ $(X_2/X_1=1.428)$ and that for the Bessel factor of $\nu=10$ $(X_2/X_1=1.398)$ is only 0.03. This gives a differential precision of these two numbers about 2.1%. Here the differential precision of a number $A$ and a number $B$ $(B>A>0)$ is defined by $(B-A)/[(A+B)/2]$. For Bessel functions of high orders, e.g., $\nu=29$ and 30, the absolute difference of their characteristic ratios is even as small as 0.004 and the corresponding differential precision is only about 0.34%. In practice, it is nearly impossible to achieve such a high detection precision in electron diffraction measurements; hence the method fails easily when applied to Bessel factors with high orders.

To overcome this limitation, we introduced a different method. By exploring two individual Bessel factor plots of neighboring orders $J^2_{|\nu|}(x)$ and $J^2_{|\nu|+1}(x)$ as shown in Fig. 2(a), it is clearly seen that Bessel factors have a mirror symmetry about $x=0$. The magnitude of the first root and the width between the pair of highest peaks of a Bessel factor increase steadily with the Bessel order $|\nu|$. The distance between the first pair of roots $W_{\mathrm{MZ1}}$ and the distance between the pair of highest peaks $W_{\mathrm{TP1}}$ are shown as a function of the Bessel order $|\nu|$ in Fig. 2(b). For a Bessel factor having a nonzero order, there is always an "intensity gap" around $x=0$, where the intensity is approaching zero. The width of the gap is also a function of the Bessel factor order. A higher-order Bessel factor has a wider intensity gap than a lower-order Bessel factor. On the other hand, the interval between the first two positive roots $(\Delta_{12})$ of a Bessel factor increases much more slowly with $|\nu|$ as shown in Fig. 2(b). Therefore, nondimensional characteristic ratios for each individual Bessel factor can be calculated by dividing $W_{\mathrm{TP1}}$ or $W_{\mathrm{MZ1}}$ by $\Delta_{12}$ as

$$R_{\mathrm{TP1}}=\frac{W_{\mathrm{TP1}}}{\Delta_{12}} \tag{2}$$

or

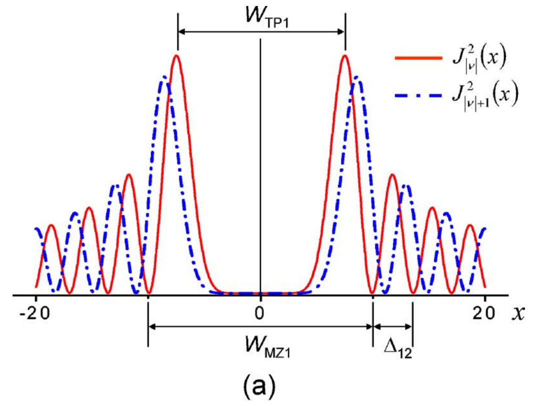


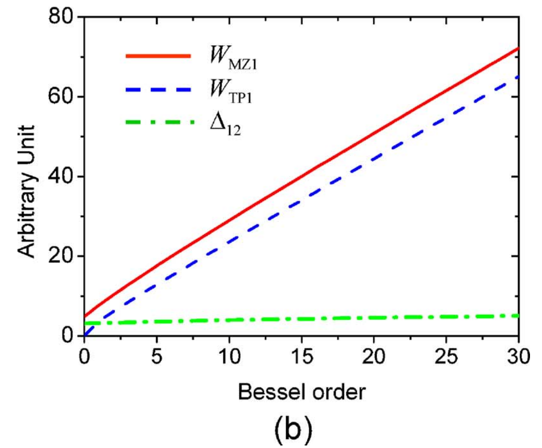


FIG. 2. (Color online) (a) Two Bessel factors with neighboring orders $J^2_{|\nu|}(x)$ and $J^2_{|\nu|+1}(x)$. A higher-order Bessel factor has a wider intensity gap than a lower order Bessel factor. (b) The distance between the first pair of roots $W_{\mathrm{MZ1}}$, and the pair of highest peaks $W_{\mathrm{TP1}}$, and the interval between the first two positive roots $\Delta_{12}$ are shown as functions of the Bessel order.

$$R_{\mathrm{MZ1}}=\frac{W_{\mathrm{MZ1}}}{\Delta_{12}}. \tag{3}$$

For example, for Bessel factors of orders $\nu=9$ and 10, $R_{\mathrm{TP1}}$ is 5.51 and 5.95, respectively, with an absolute difference of 0.44. Likewise, $R_{\mathrm{MZ1}}$ is 6.87 and 7.31, also with a difference of 0.44. The corresponding differential precision for distinguishing these two Bessel factors is then 7.9% when using $R_{\mathrm{TP1}}$, or 6.2% when using $R_{\mathrm{MZ1}}$. In the case of Bessel factors of higher orders $\nu=29$ and 30, the absolute differences of their $R_{\mathrm{TP1}}$ ratios and of their $R_{\mathrm{MZ1}}$ ratios are both as large as 0.31, with differential precisions being 2.4% and 2.2%, respectively. Therefore, the introduction of $R_{\mathrm{TP1}}$ and $R_{\mathrm{MZ1}}$ allows considerably higher differential precisions for distinguishing adjacent Bessel factors, thus allowing the use of layer lines dominated by high-order Bessel functions.

Characteristic ratios $R_{\mathrm{TP1}}$ and $R_{\mathrm{MZ1}}$ for Bessel factors of orders from $\nu=0$ to 30 have been tabulated and listed in Table I. For reference, the position ratio of the first two (positive) peaks $(X_2/X_1)$ of the corresponding Bessel factor introduced in Ref. 11 is also included in Table I. By comparing the ratios measured from the intensity profiles along diffraction layer lines with those listed in Table I, Bessel orders can immediately be recognized, which are then ascribed to

TABLE I. Characteristic ratios $R_{TP1}$, $R_{MZ1}$, and $X_2/X_1$ for Bessel factors of orders from $\nu=0$ to 30.

| $\|\nu\|$ | $R_{TP1}$ | $R_{MZ1}$ | $\frac{X_2}{X_1}$ [a] |
|---|---|---|---|
| 1 | 1.156 | 2.407 | 2.892 |
| 2 | 1.859 | 3.130 | 2.197 |
| 3 | 2.485 | 3.774 | 1.907 |
| 4 | 3.061 | 4.366 | 1.751 |
| 5 | 3.600 | 4.918 | 1.639 |
| 6 | 4.106 | 5.440 | 1.565 |
| 7 | 4.595 | 5.937 | 1.507 |
| 8 | 5.062 | 6.413 | 1.465 |
| 9 | 5.511 | 6.871 | 1.428 |
| 10 | 5.947 | 7.315 | 1.398 |
| 11 | 6.373 | 7.744 | 1.373 |
| 12 | 6.784 | 8.162 | 1.350 |
| 13 | 7.187 | 8.569 | 1.332 |
| 14 | 7.581 | 8.966 | 1.315 |
| 15 | 7.963 | 9.355 | 1.301 |
| 16 | 8.338 | 9.735 | 1.287 |
| 17 | 8.707 | 10.11 | 1.275 |
| 18 | 9.070 | 10.47 | 1.266 |
| 19 | 9.427 | 10.83 | 1.256 |
| 20 | 9.779 | 11.19 | 1.247 |
| 21 | 10.12 | 11.53 | 1.239 |
| 22 | 10.46 | 11.88 | 1.232 |
| 23 | 10.80 | 12.21 | 1.226 |
| 24 | 11.13 | 12.55 | 1.218 |
| 25 | 11.46 | 12.87 | 1.211 |
| 26 | 11.78 | 13.20 | 1.206 |
| 27 | 12.10 | 13.52 | 1.201 |
| 28 | 12.41 | 13.83 | 1.196 |
| 29 | 12.72 | 14.15 | 1.192 |
| 30 | 13.03 | 14.46 | 1.188 |

[a]Reference 11.

the chiral indices of the nanotube. By using several combinations of $R_{TP1}$ and $R_{MZ1}$ from different layer line measurements to complement and verify each other in a measurement, a high level of confidence can be achieved.

Though the above-described method has obvious advantages over that proposed by Liu and Qin,[11] neither method takes into account the effect of nanotube tilting with respect to the electron beam. This may be a vital restriction in practical applications of both methods since one cannot expect a carbon nanotube to be exactly under the normal-incident condition. Thus, it is crucial to elucidate the effect of the tilt on the validity of the methods.

An electron diffraction pattern is a planar cut of the carbon nanotube's counterpart in reciprocal space by the Ewald sphere which is approximated to be a plane for high-energy electrons. Since the SWCNT is a one-dimensional periodical structure, its reciprocal counterpart structure is a series of

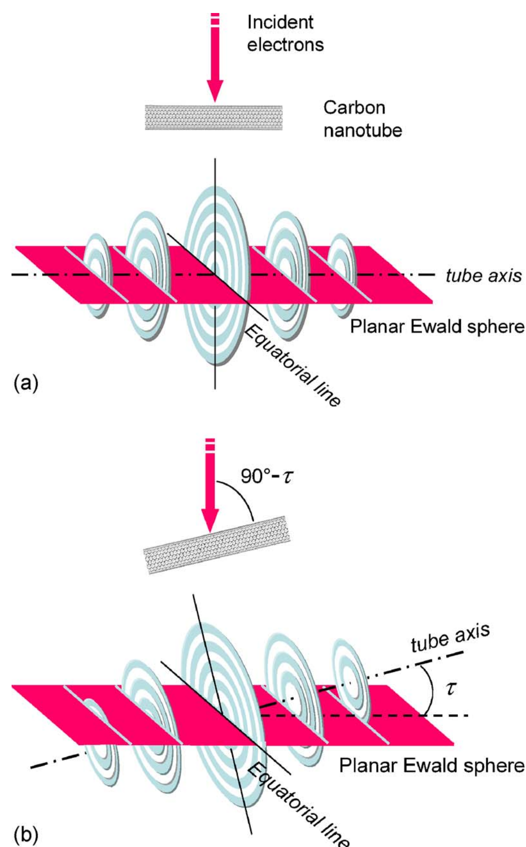


FIG. 3. (Color online) Planar cuts of the reciprocal counterpart of a SWCNT by the Ewald sphere which is approximated to be a plane for high-energy electrons: (a) in normal incidence; (b) when the tube is tilted by an angle $\tau$ with respect to the incident electron beam.

discrete diffraction disks, which are parallel to each other but perpendicular to the tube axis.[13,16,21] In normal incidence as shown in Fig. 3(a), the intersection lines of the diffraction disks by the planar Ewald sphere, i.e., the layer lines in the diffraction pattern, are crossing the disk centers. The radial intensity distribution along an intersection line is, then, described by a Bessel factor with a particular order as has been shown previously.

When the nanotube is tilted with respect to the incident electron beam [Fig. 3(b)], the reciprocal structure of the nanotube is tilted accordingly as if it was rigidly bound to the tube. In this situation, the intersection lines are no longer passing through the disk centers except at the central equatorial line. In such a situation, any nonequatorial layer line shows an intensity profile that varies significantly with the tilt angle and, therefore, cannot be simply interpreted as a Bessel factor with an integer order that is supposed to be directly related to the chiral indices of the nanotube.

## IV. RESULTS

As an example, Fig. 4(a) presents a simulated normal-incidence diffraction pattern of a chiral (40,5) single-walled carbon nanotube. One of the diffraction disks corresponding to the (0,1) reflection of the tube is shown in Fig. 4(b). The

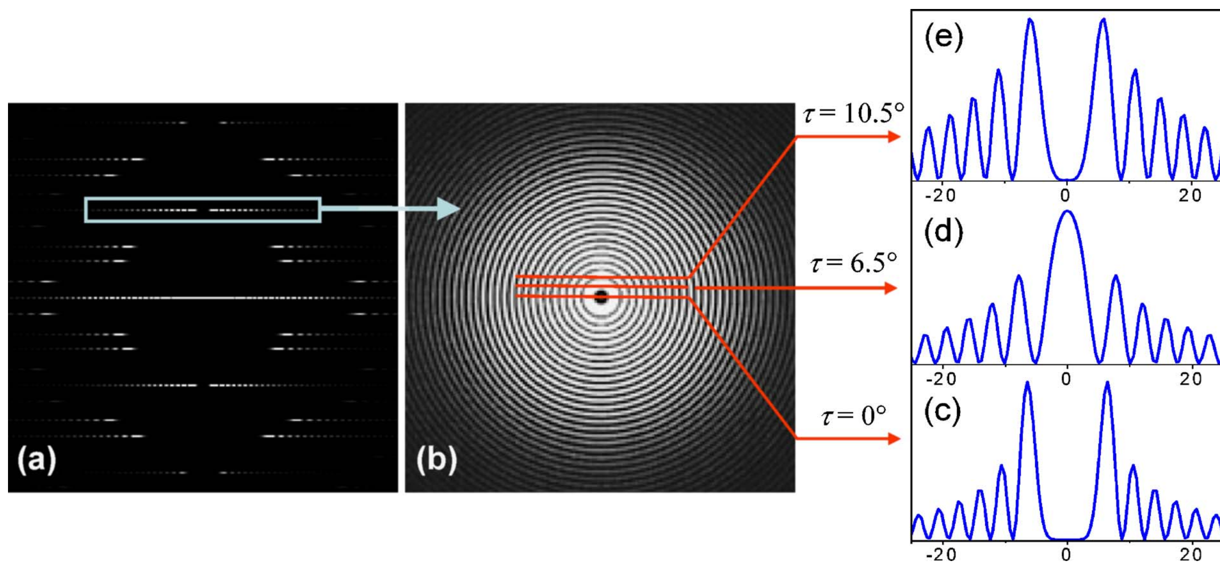


FIG. 4. (Color online) (a) A simulated diffraction pattern of a chiral (40,5) SWCNT. (b) The diffraction disk for the corresponding (0,1) reflection. (The diffraction disk for the (0,1) reflection of the (40,5) SWCNT shown in (b) is duplicated from Ref. 21.) (c)–(e) The intensity profiles along the secant lines for tilts at $\tau$=0°, 6.5°, and 10.5°, respectively.

dependence of the secant line's position in the disk, hence the intensity distribution along the intersection line on the tilt angle is clearly shown in Figs. 4(c)–4(e). One can visualize from Fig. 4(b) that, when the tilt angle is small, the width of the intensity gap of the layer line decreases gradually as the tilt angle increases until a critical angle, which is defined when the secant line reaches the tangent line at the innermost dark circle of the diffraction disk. At this angle, the pair of strongest peaks along a layer line merges into a single peak on the meridian [Fig. 4(d)]. As the tilt angle progressively increases, the above-mentioned single peak starts to split up into two [Fig. 4(e)] with an intensity gap depending on the tilt angle and on the intrinsic intensity distribution of the diffraction disk. Therefore, quantitative interpretation of intensity distribution along nonequatorial layer lines in the diffraction pattern is problematic before the tilt angle is known.

In order to further demonstrate the considerable effect of the tube tilt on the $(n,m)$ determination, Fig. 5 shows three simulated electron diffraction patterns of a (29,2) SWCNT at tilt angles of (a) 0°, (b) 3°, and (c) 6°, respectively. The intensity profiles of the layer lines passing through (1,0) and (0,1) reflections (as labeled $L_1$ and $L_2$, respectively) from all three patterns are shown in Figs. 5(d)–5(i). It is immediately apparent that the $L_1$ layerline has a seemingly wider intensity gap than the $L_2$ layer line due to the fact that, in this case, the $L_1$ layer line is dominated by a Bessel function of order $\nu_n$=29, and the $L_2$ layer line by a Bessel function of order $\nu_m$=2.

Let us start with the diffraction pattern at a tilt angle of 0°. In Table II(a) are listed the ratios $R_{\text{TP1}}$ and $R_{\text{MZ1}}$ calculated from both $L_1$ and $L_2$ layer lines in Fig. 5(a). By comparing them with their nearest characteristic values in Table I, the Bessel orders are directly recognizable as $\nu_n$=29 and $\nu_m$=2 accordingly for $L_1$ and $L_2$ layer lines with little ambiguity. For comparison, the position ratios $X_2/X_1$ (Ref. 11) of the first two positive peaks of both $L_1$ and $L_2$ layer lines are also measured and listed in the last row of Table II(a). With the $X_2/X_1$ value measured from the $L_2$ layer line, $\nu_m$=2 is well identified, though the error is rather large. However, from the $L_1$ layer line, $\nu_m$ is obviously closer to 28, rather than its true value of 29.

When the tube is tilted by 3° away from the normal incidence, there is no perceptible change in the $L_1$ layer line to the eye; but the change in the $L_2$ layer line with a narrow intensity gap is obvious [Fig. 5(b)]. The distance between the pair of strongest peaks along the $L_2$ layer line considerably narrows and the peaks start to merge [Fig. 5(e)]. The characteristic ratios measured from $L_1$ and $L_2$ layer lines at a 3° tilt is given in Table II(b). From the $L_1$ layer line, $\nu_n$ can still be recognized as 29 with good confidence based on either $R_{\text{TP1}}$ or $R_{\text{MZ1}}$. However, the $R_{\text{TP1}}$ and $R_{\text{MZ1}}$ values measured from the $L_2$ layer line appear almost exactly between the corresponding characteristic values for $\nu_m$=1 and 2, thus selection of the true chiral indices becomes uncertain.

As the tilt angle gradually increases to the critical angle, about 6° for the $L_2$ layer line [Fig. 5(c)], the pair of strongest peaks merges into one single peak on the meridian as shown in Fig. 5(f). In this situation, the intensity profile along the $L_2$ layer line looks, incorrectly, like a Bessel factor of zero order, hence determination of the Bessel order from the $L_2$ layer line fails. However, by using the $L_1$ layer line that has a wider intensity gap around its center, the measured ratios $R_{\text{TP1}}$ or $R_{\text{MZ1}}$ remain valid for determining $\nu_n$=29 unambiguously [Table II(c)].

Based on the above results, it is evident that the diffraction layer lines having wide intensity gaps (corresponding to Bessel factors of high orders) suffer less from the effect of the tilt, and hence tolerate higher tilt angles, than those having narrow intensity gaps (corresponding to Bessel factors of low orders). Consequently, they are particularly favored for $(n,m)$ evaluations. It is interesting to note that, when using the peak position ratio $X_2/X_1$ (Ref. 11) for analysis of the $L_1$

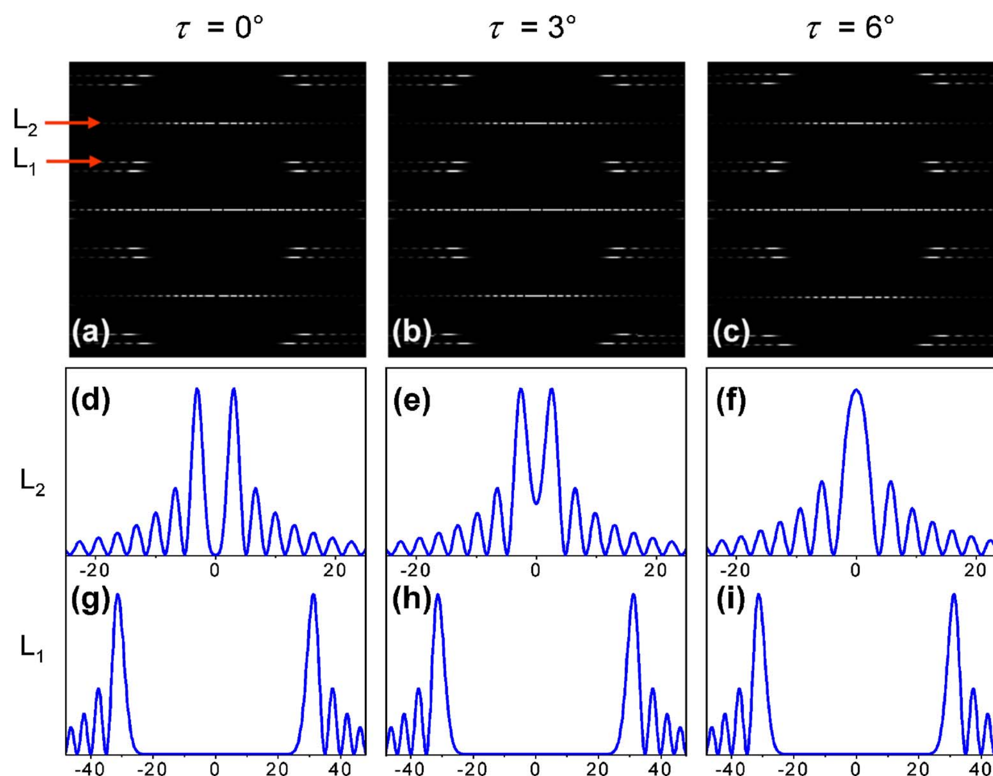


FIG. 5. (Color online) Simulated electron diffraction patterns of a (29,2) SWCNT, with tilt angles of (a) 0°, (b) 3°, and (c) 6°, respectively. (d)–(i) Intensity profiles along layer lines $L_1$ and $L_2$ in the diffraction patterns of respective tilt angles.

layer line, an incorrect determination of the Bessel order $\nu_n=18$ is attained in all situations of 0°, 3°, and 6° tilt. The reason for this deviation is mainly because, for such a high-order Bessel factor, the differential precision of its adjacent $X_2/X_1$ ratios is so small that correctly identifying the Bessel factor is extremely sensitive to measurement errors. On the other hand, as the $\nu_n$ determination gives the same result in all three examined tilt cases, it is further demonstrated that the layer line having a wide intensity gap is little affected by small tilt angles.

TABLE II. Ratios $R_{\mathrm{TP1}}$ and $R_{\mathrm{MZ1}}$ determined from $L_1$ and $L_2$ layer lines on the diffraction patterns of a (29, 2) nanotube, and the corresponding best fit values of the Bessel orders.

| | $L_1$ layer line | | $L_2$ layer line | |
|---|---|---|---|---|
| Ratios | Determined values | $\nu_n$ of the best fit | Determined values | $\nu_m$ of the best fit |
| (a) In normal incidence | | | | |
| $R_{\mathrm{TP1}}$ | 12.70 | 29 | 1.804 | 2 |
| $R_{\mathrm{MZ1}}$ | 14.23 | 29 | 3.073 | 2 |
| $\frac{X_2}{X_1}$ [a] | 1.195 | 28 | 2.248 | 2 |
| (b) At a tilt angle of 3° | | | | |
| $R_{\mathrm{TP1}}$ | 12.70 | 29 | 1.526 | 1 or 2 |
| $R_{\mathrm{MZ1}}$ | 14.23 | 29 | 2.927 | 1 or 2 |
| $\frac{X_2}{X_1}$ [a] | 1.197 | 28 | 2.565 | 1 or 2 |
| (c) At a tilt angle of 6° | | | | |
| $R_{\mathrm{TP1}}$ | 12.70 | 29 | | |
| $R_{\mathrm{MZ1}}$ | 14.19 | 29 | 1.910 | |
| $\frac{X_2}{X_1}$ [a] | 1.195 | 28 | | |

[a]Reference 11.

The proposed method has been applied to determine the chiral indices of single-walled carbon nanotubes synthesized by an aerosol method using ethanol as a carbon precursor, and iron aerosol nanoparticles as catalysts.[23] Figure 6 shows (a) a high-resolution TEM image of an individual SWCNT and (b) its corresponding EDP, both of which were taken by a Philips CM200-FEG TEM operating at the highest possible accelerating voltage of 200 kV to reduce the Ewald sphere curvature effect. The microscope is equipped with a Gatan 794 multiscan CCD camera (1 k × 1 k) for digital recording. The layer lines passing through (0,1) and (1,1) reflections as labeled $L_1$ and $L_2$ in Fig. 6(b) are employed for $(n,m)$ determination. The intensity profiles along $L_1$ and $L_2$ layer lines are shown in Figs. 6(c) and 6(d), respectively. From the $L_1$ layer line, $R_{\mathrm{TP1}}$ is calculated to be 5.92, based on which the chiral index $m$ is confidently identified as 10. Likewise, from the $L_2$ layer line $R_{\mathrm{TP1}}$ is calculated to be 7.30, giving the value $n-m=13$, thus $n$ is recognized to be 23. This (23,10) tube is a semiconducting nanotube of diameter $D_0$ =2.29 nm, and chiral angle $\alpha=17.2°$. The result coincides with that determined from the same diffraction pattern but by an independent technique.[24] It is worth remarking that the same nanotube was previously determined to be a (21,9) metallic nanotube[22,25] by the preliminary method based on $(D_0,\alpha)$ determination.[10] A direct comparison shows that the

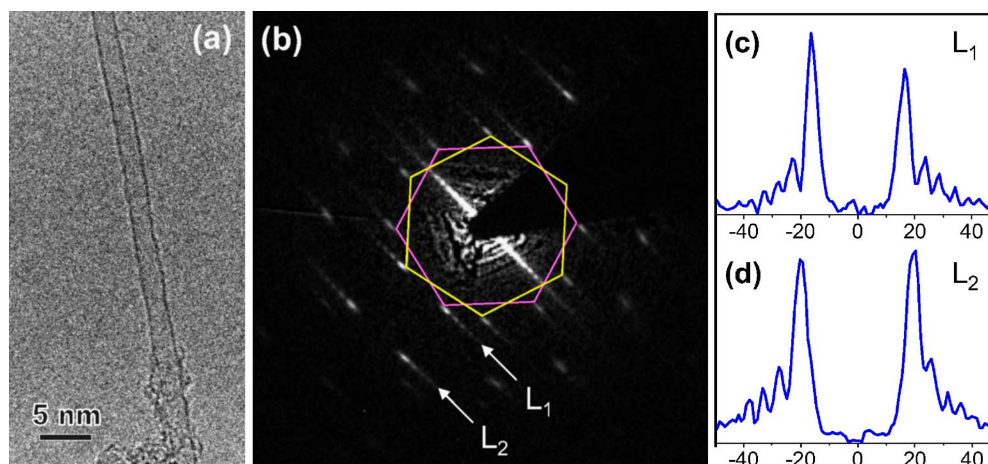


FIG. 6. (Color online) (a) A high-resolution TEM image of an individual SWCNT. (b) The corresponding experimental electron diffraction pattern. (c)–(d) Intensity profiles along the $L_1$ and $L_2$ layer lines indicated in (b).

difference between the chiral angles of the (23,10) tube and the (21,9) tube is just 0.19°, but the diameters differ from each other by 10%. Calibration error due to neglecting the tilt effect accounts for the large error in the earlier evaluation of the tube diameter.

## V. CONCLUSIONS

In this paper, we present a Bessel-function-based method for direct determination of chiral indices of SWCNTs from their electron diffraction patterns. In a normal-incidence electron diffraction pattern of a SWCNT, the orders of Bessel factors for the diffraction layer lines are directly associated with the chiral indices of the nanotube. An effective approach has been introduced with the purpose of retrieving the structural $(n,m)$ indices of the nanotube by confidently evaluating the intensity modulations along diffraction layer lines. This method noticeably improves precision and makes high-order Bessel function analysis feasible.

The effect of nanotube titling on the validity of the method for $(n,m)$ determination has been critically evaluated. It is shown that the intensity distribution along a nonequatorial layer line is sensitive to the tilt of the tube. Thus, a direct comparison of layer-line intensity distributions between an experimental pattern and a simulated pattern is ambiguous before the tilt angle is determined. Strictly speaking, when the tilt angle is nonzero, the intensity profile along a certain nonequatorial layer line in the EDP of a SWCNT cannot be simply described by a Bessel function with an integer order.

On the other hand, we show that diffraction layer lines having wider intensity gaps, which correspond to high-order Bessel functions, are favored for $(n,m)$ characterization because they suffer less from the tilting effect, hence tolerate higher tilt angles than those having narrower intensity gaps. The method introduced in this work allows these less sensitive diffracted layer lines to be used, thereby, dramatically improves the chiral index determination of SWCNTs. The method is also important when electron diffraction patterns are of relatively low pixel resolution. Moreover, the technique can be extended to the structural analysis of double-walled carbon nanotubes, since the method is independent of information from the central equatorial layer line.

The effectiveness of the proposed method has been demonstrated by a tangible example. A single-walled carbon nanotube, which was previously evaluated to be a metallic (21,9) tube by using the primitive diffraction analysis method based on $(D_0,\alpha)$ determination, is ascertained to be a (23,10) semiconducting nanotube determined from the same electron diffraction pattern by the present method. The results have been reassured by an interpretation of the same EDP with another independent technique.

## ACKNOWLEDGMENTS

The authors thank Ph. Lambin for providing us with the FORTRAN code of their DIFFRACT program for the simulation of electron diffraction patterns of SWCNTs in this paper. Hua Jiang is grateful to Ph. Lambin and M. Kociak for fruitful discussions. This work is supported by the VTT, TEKES, and the Academy of Finland.

*Corresponding author. FAX: +358 20 7227021; Email address: hua.jiang@vtt.fi

†Corresponding author. FAX: +358 20 7227021; Email address: esko.kauppinen@vtt.fi

[1] S. Iijima and T. Ichihashi, Nature (London) **363**, 603 (1993).

[2] R. Saito, G. Dresselhaus, and M. S. Dresselhaus, *Physical Properties of Carbon Nanotubes* (Imperial College Press, London, 1998).

[3] N. Hamada, S. I. Sawada, and A. Oshiyama, Phys. Rev. Lett. **68**, 1579 (1992).

[4] J. Maultzsch, H. Telg, S. Reich, and C. Thomsen, Phys. Rev. B **72**, 205438 (2005).

[5] A. Jorio, R. Saito, J. H. Hafner, C. M. Lieber, M. Hunter, T. McClure, G. Dresselhaus, and M. S. Dresselhaus, Phys. Rev. Lett. **86**, 1118 (2001).

[6] S. M. Bachilo, M. S. Strano, C. Kittrell, R. H. Hauge, R. E. Smalley, and R. B. Weisman, Science **298**, 2361 (2002).

[7] J. W. G. Wildöer, L. C. Venema, A. G. Rinzler, R. E. Smalley, and C. Dekker, Nature (London) **391**, 59 (1998).

[8] T. W. Odom, J. L. Huang, P. Kim, and C. M. Lieber, Nature (London) **391**, 62 (1998).

[9] A. Hashimoto, K. Suenaga, K. Urita, T. Shimada, T. Sugai, S. Bandow, H. Shinohara, and S. Iijima, Phys. Rev. Lett. **94**, 045504 (2005).

[10] M. Gao, J. M. Zuo, R. D. Twesten, I. Petrov, L. A. Nagahara, and R. Zhang, Appl. Phys. Lett. **82**, 2703 (2003).

[11] Z. Liu and L.-C. Qin, Chem. Phys. Lett. **408**, 75 (2005).

[12] Z. Liu, Q. Zhang, and L.-C. Qin, Phys. Rev. B **71**, 245413 (2005).

[13] J. C. Meyer, M. Paillet, G. S. Duesberg, and S. Roth, Ultramicroscopy **106**, 176 (2006).

[14] M. Kociak, K. Suenaga, K. Hirahara, Y. Saito, T. Nakahira, and S. Iijima, Phys. Rev. Lett. **89**, 155501 (2002).

[15] M. Kociak, K. Hirahara, K. Suenaga, and S. Iijima, Eur. Phys. J. B **32**, 457 (2003).

[16] K. Hirahara, S. Bandow, H. Kataura, M. Kociak, and S. Iijima, Phys. Rev. B **70**, 205422 (2004).

[17] J. C. Meyer (private communication).

[18] L.-C. Qin, J. Mater. Res. **9**, 2450 (1994).

[19] L.-C. Qin, Chem. Phys. Lett. **297**, 23 (1998).

[20] Ph. Lambin and A. A. Lucas, Phys. Rev. B **56**, 3571 (1997).

[21] S. Amelinckx, A. A. Lucas, and Ph. Lambin, Rep. Prog. Phys. **62**, 1471 (1999).

[22] A. A. Lucas and Ph. Lambin, Rep. Prog. Phys. **68**, 1181 (2005).

[23] A. G. Nasibulin, A. Moisala, D. P. Brown, H. Jiang, and E. I. Kauppinen, Chem. Phys. Lett. **402**, 227 (2005).

[24] H. Jiang, A. G. Nasibulin, D. P. Brown, and E. I. Kauppinen, Carbon (to be published).

[25] H. Jiang, A. G. Nasibulin, A. Moisala, and E. I. Kauppinen, *Proceedings of the 13th European Microscopy Congress, Antwerp*, 2004, Vol. II, p. 235.